Measuring (Oblique) Wave Run-Up and Overtopping with Laser Scanners

Oosterlo, Patrick; Hofland, Bas; van der Meer, Jentsje; Overduin, Maarten; Steendam, Gosse Jan; Nieuwenhuis, Jan-Willem; van Vledder, Gerbrant; Steetzel, Henk; Reneerkens, Michiel

DOI
10.18451/978-3-939230-64-9_045

Publication date
2019

Document Version
Final published version

Published in
Coastal Structures 2019

Citation (APA)
Oosterlo, P., Hofland, B., van der Meer, J., Overduin, M., Steendam, G. J., Nieuwenhuis, J.-W., van Vledder, G., Steetzel, H., & Reneerkens, M. (2019). Measuring (Oblique) Wave Run-Up and Overtopping with Laser Scanners. In N. Goseberg, & T. Schlurmann (Eds.), *Coastal Structures 2019* Bundesanstalt für Wasserbau. https://doi.org/10.18451/978-3-939230-64-9_045

Conference Paper, Published Version

Oosterlo, Patrick; Hofland, Bas; van der Meer, Jentsje; Overduin, Maarten; Steendam, Gosse Jan; Nieuwenhuis, Jan-Willem; van Vledder, Gerbrant; Steetzel, Henk; Reneerkens, Michiel

Measuring (Oblique) Wave Run-Up and Overtopping with Laser Scanners

Coastal Structures 2019 - Nils Goseberg, Torsten Schlurmann (eds) - © 2019 Bundesanstalt für Wasserbau
ISBN 978-3-939230-64-9 (Online) - DOI: 10.18451/978-3-939230-64-9_045

Measuring (Oblique) Wave Run-Up and Overtopping with Laser Scanners

P. Oosterlo[1], B. Hofland[1], J.W. van der Meer[1,2,3], M. J. Overduin[4], G. J. Steendam[4], J. W. Nieuwenhuis[5], G. Ph. van Vledder[1,6], H. Steetzel[7], M. Reneerkens[8]
[1]*Delft University of Technology, Delft, The Netherlands; P.Oosterlo@tudelft.nl*
[2]*Van der Meer Consulting BV, Akkrum, The Netherlands*
[3]*IHE Delft, Delft, The Netherlands*
[4]*Infram Hydren, Maarn, The Netherlands*
[5]*Waterschap Noorderzijlvest, Groningen, The Netherlands*
[6]*Van Vledder Consulting, Olst, The Netherlands*
[7]*Arcadis, Zwolle, The Netherlands*
[8]*Aqua Vision, Utrecht, The Netherlands*

Abstract: Wave overtopping is commonly measured using overtopping tanks. In this paper, an alternative system is developed by using two laser scanners. It measures wave run-up, as well as layer thicknesses and front velocities, both during normally and obliquely incident waves on a dike in the field. The paper considers the first field validation tests with the system, with normal and oblique waves generated by the wave run-up simulator on a grass dike slope. Furthermore, a range of environmental conditions are simulated, to determine the robustness of the system. From the measured distance and reflection, the run-up is determined, which corresponds well to the observed run-up. From the data, the layer thickness and front velocity are determined as well. Layer thicknesses and front velocities are determined reliably with the laser scanners. Also, the (virtual) wave overtopping discharge can be calculated, which corresponds well with the most commonly used overtopping equations.

Keywords: Laser scanner, LIDAR, wave run-up, wave overtopping, layer thickness, front velocity, dike grass cover, field measurements

1 Introduction

The Eems-Dollard estuary in the north of the Netherlands is a highly complex estuary with deep channels and tidal flats, which is part of the Wadden Sea. A particular aspect for this area is that the dike design conditions often are characterized by very obliquely incident waves, up to 80° relative to the dike normal. As the reliability of the models as used for the Dutch dike safety assessment is unknown for such conditions, an extensive field measurement project is performed in this estuary for a period of 12 years. The measurements started in 2018, measuring wind, water levels, currents, waves and wave run-up and overtopping.

In the project, wave overtopping is measured with two innovative wave overtopping tanks built into the dike. This is a robust method to measure wave overtopping, but fixed in one place.

An alternative and possibly more flexible solution than a fixed overtopping box is being developed using two terrestrial laser scanners (LIDARs) to measure wave run-up and the front velocities and layer thicknesses at a dike in field situations with oblique wave attack. From these measurements the virtual wave overtopping can be calculated at any virtual crest level, which is the objective of this paper. The present paper describes the design, set-up and processing, analysis and validation with physically simulated normally and obliquely incident waves on an actual grass dike slope. First, the approach and set-up of the system are presented and the set-up of the tests is given. After that, the post-processing and analysis are described. This is followed by the validation of the measured parameters. An outlook is given on the next steps in this study. If the validation is positive, the system will be placed on a dike for 3 years to measure wave run-up and to calculate the overtopping for severe winter storms additional to the measurements with overtopping tanks.

2 Approach and system set-up

Laser scanners are often used for terrestrial measurements, but have also been used to measure the water surface or waves (Blenkinsopp et al., 2010; Allis et al., 2011; Streicher et al., 2013) and recently also to measure wave run-up (Vousdoukas et al., 2014; Hofland et al., 2015). The system uses two SICK LMS511pro HR laser scanners, a relatively cheap laser scanner that uses a near-infrared (905 nm) laser beam and which has been the most commonly used laser scanner in the previous studies. The system set-up was based on Hofland et al. (2015), but now consists of a set of two synchronized laser scanners instead of one, attached to an easily relocatable pole. See Fig. 1 for the validation set-up at a dike in Friesland, the Netherlands. The laser scanners measure the distance (*R)* to a surface by measuring the time that the reflection of a laser pulse takes to reach the scanner again. The reflected signal intensity (*RSSI)* is also measured, which provides information on the type of surface (e.g. wet or dry). The scanners measure the development of the water surface profile in time with 50 Hz, providing an accurate temporal evolution of the profile. The two laser scanners each scan a line with a certain distance from each other, in this case running from the dike toe to the crest (red and blue lines in right panel of Fig. 1). Two laser scanners are used, to also be able to efficiently measure directional information of the waves. To this end the scanners are synchronised. The height of the laser scanners and the distance between both scanned lines are adjustable.

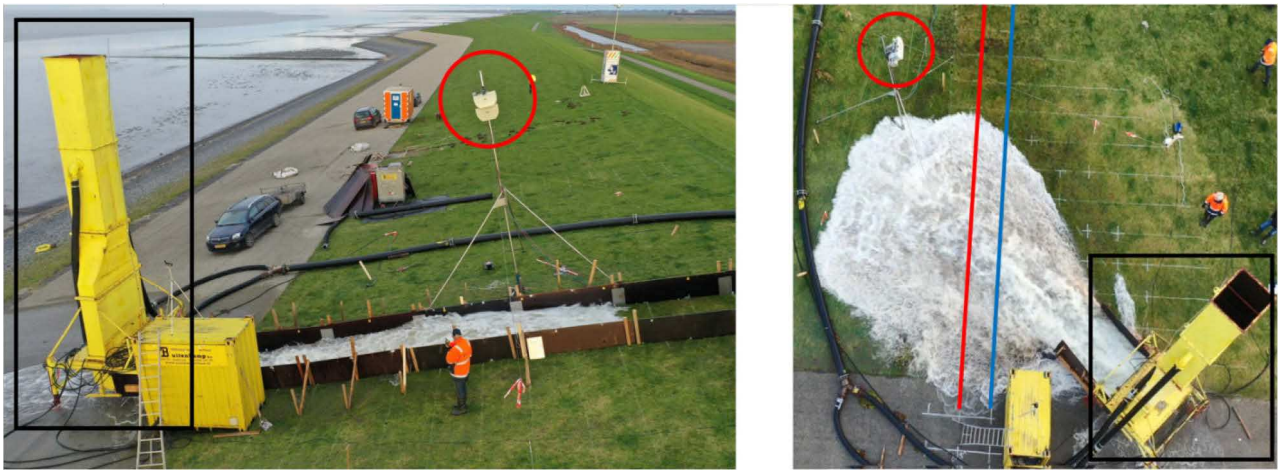

Fig. 1. Left: Laser scanner system (red circle) and run-up simulator (black rectangle) during tests with normally incident waves. Right: Top view during obliquely incident waves (scan lines indicated by red and blue lines).

The system was first tested with waves generated by the wave run-up simulator (Van der Meer, 2011) on the grass slope of the dike. The laser scanners were placed perpendicular to the local slope at heights of 5.17 and 5.50 m above the slope. Complicating factors compared to the previous (laboratory) research on concrete or wooden slopes are e.g. the convex shape of the dike slope, which means that the slope angle is not the same everywhere, wave-induced erosion of the grass slope, the blades of grass, which might obfuscate a thin layer of water, as well as infiltration of water into the slope.

During this first system test, multiple tests were performed. Incident ‘waves’ (released volumes, hereafter referred to as waves) were simulated using the wave run-up simulator, which consists of a vertical tank filled with water to a certain level. By quickly opening the bottom of the tank, the tank drains simulating an individual wave running up the slope.

First, tests were performed for normally incident waves (tests 1 to 13), where 7 different conditions were repeated three times to obtain increased statistical reliability. Hence, in total 21 waves were simulated by using the different filling levels of the wave run-up simulator (1 to 7 m). With these normally incident waves, the influence of a large range of environmental conditions (e.g. producing artificial wind and rain) and laser scanner parameters were tested and calibrated. For test 1a, 100 normally incident random volumes were generated, to be able to assess the performance of the system in e.g. predicting the wave run-up and overtopping. The time series of filling levels of the simulator were derived from a nearshore significant wave height of 2 m and a peak period of 5.7 s.

After that, the wave run-up simulator was placed under an angle with the dike normal. With this set-up, obliquely incident waves under an angle of 45° were generated and tests were performed to

determine the ideal distance between the scanned lines and distance from the simulator to the scanned lines. Tests 14 to 17 were used, which contain 3 times 6 waves (filling levels from 2 to 7 m). Test 17a again consisted of 100 randomly generated waves, to assess the system for oblique run-up and overtopping.

For the validation, a relation between the filling level of the simulator and the resulting run-up height was determined from several visually observed run-up heights for this specific location. With this relation, the theoretical run-up level can be determined for each filling level. Run-up heights and front velocities were also determined from videos. Layer thicknesses and velocities near the ground were measured with 'surf boards', floaters from which the layer thickness can be determined and paddle wheels, impellers that measure the velocities near the ground (see e.g. Van der Meer et al. (2010)).

3 Data processing

3.1 Calibration

Before the start of the tests, the exact positions of the laser scanners were determined by noting all the dimensions of the system and determining the exact locations of the laser lines with an alignment bar. This is a bar with several infrared detectors and LEDs that light up when infrared light is detected. Several scans were made with two wooden beams at known locations on the dike slope, to calibrate the lasers before the actual measurements.

The first step in the data processing was to convert the raw data files to the format of MATLAB, the software used for the analysis. The relevant data consists of the scanner serial number, the start angle at which the laser scanner starts measuring, the angular resolution, the time, the measured distance R in polar coordinates of the first, last or all five echoes and the RSSI (Received Signal Strength Indicator) values of the first, last or all five echoes. The RSSI is given as a dimensionless value between 0 and 255. After that, the orientation of the lasers was determined and the measured distances (in polar coordinates) were converted to x and z coordinates in m, see Fig. 2. For this, it was important that the laser scanners were placed perpendicular to the slope and that the local slope angle (since the slope angle differs along the slope) at the location of the pole was accurately known. Using the calibration data with the known locations of the wooden beams, the exact locations of the laser scanners were determined. The maximum difference between the known x-coordinates of the beams and the x-coordinates of the beams according to the laser scanners was 5 cm, which is of the same order of magnitude as the scan resolution and laser footprint. The laser data were corrected for this and next the dry slope resulting from the laser scanners was compared to the slope as measured with measurement tape and laser distance meter. Here, the maximum difference in z-coordinate was 5 cm as well, which is highly accurate considering the convex shape of the dike slope and the grass blades.

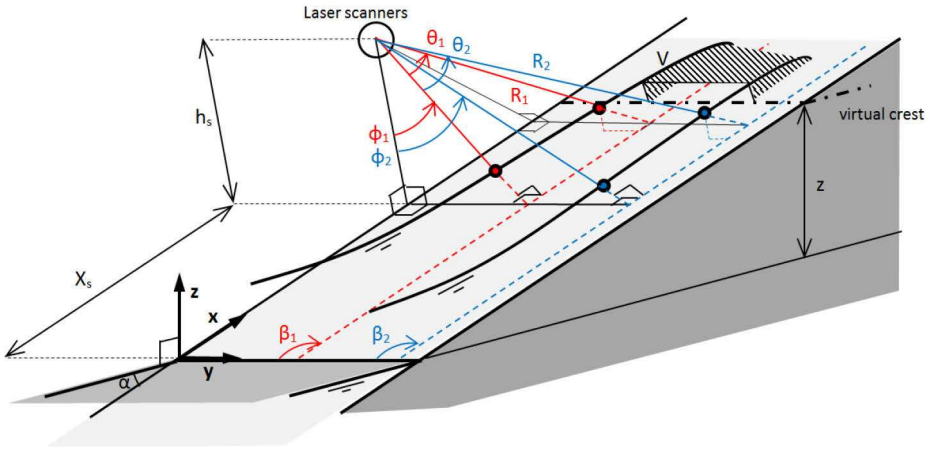

Fig. 2. Schematised set-up with two laser scanners. Set-up based on Hofland et al. (2015), but with two laser scanners. Scan lines (red and blue dashed lines), scanned points on water surface (red and blue dots) indicated. R is the scanned distance [m], θ the scan angle [°], ϕ the slant angle [°], β a correction in case the scanned line does not run straight along the slope [°]. h_s the height of the laser scanners [m], x_s the x-coordinate of the laser scanners [m], α the slope angle [°]. V is a virtual overtopping volume [m^3].

3.2 Data quality

The data were then further processed. In case all five echoes were recorded, the maximum distance of all echoes was taken, as well as the maximum RSSI value, to partly filter out e.g. rain or fog, as these give smaller distances and RSSI values. If no clear reflection was detected by the scanner, a NaN (Not a Number) was recorded. The percentage of valid measurements at a certain location gives an indication of the quality of the measurement. For all tests, the minima of these percentages were very high (>99%). The data were then filtered in space and time, using a five-point median filter to remove outliers. The percentage of data points that change more than 1 cm or more than 5 cm due to the filtering are both indicators for the quality of the measurement. Over all tests the maximum percentage of points that changed more than 1 cm was around 10%, the maximum percentage of points that changed more than 5 cm was in the order of 1%.

Then the data were interpolated in space, with the constant spacing being the densest laser data spacing, 3 cm in this case. The dry slope was then determined for each test separately by taking the first ten seconds of a test, since erosion started to occur directly in front of the wave run-up simulator. Next, the layer thickness was determined by subtracting the dry slope from the measured slope at a certain moment. These data were corrected by removing negative layer thicknesses, as well as layer thicknesses larger than 1.5 m, to filter out rain or a person standing in the laser beam. The layer thickness was then filtered further by removing large (>0.5 m) local (in 1 time or space step) differences in layer thickness, which were e.g. caused by raindrops. Layer thicknesses smaller than a certain threshold were then removed to remove noise from the signal and prevent the detection of unrealistically high run-up values. This threshold was determined separately for each test and is another indicator of the quality of the measurement. Finally, if a valid layer thickness >20 cm occurred higher on the slope after more than 40 straight NaN values, these values were also removed, as they were caused by someone or something standing in the laser beam. A similar procedure was followed for the RSSI: a large difference (>100) in one time or space step was removed, and for each test a different threshold value was used to prevent unrealistically high run-ups, and valid values after 40 or more NaNs were removed as well. The run-up could then be determined from the resulting layer thickness and RSSI time series by finding the highest location on the slope where z_{runup}-z_{dry}>$z_{threshold}$ and $RSSI_{runup}$-$RSSI_{dry}$>$RSSI_{threshold}$.

4 Results and Analysis

4.1 Results and analysis of laser scanner settings and environmental conditions

The percentage of valid measurements, the percentage of points that changed more than 1 or 5 cm by the median filters, the chosen layer thickness threshold and RSSI threshold are all indicators of the quality of a measurement and are used here to assess the influence of different environmental conditions and the performance of different laser scanner settings during these conditions.

For all tests (thus all different environmental conditions and laser settings), the minimum percentage of valid measurements at a certain location was very high, larger than 99%, which means that in general the data should be reliable. Of the tests without rain or vibrations, the tests with the first echo, last echo and particle filter seemed to give the best results, as they had the smallest percentages of filtered points (<6% for 1 cm change and <0.4% for 5 cm change). Furthermore, these tests use the lowest layer thickness and RSSI thresholds (0.01 m and 5, respectively). This very low threshold value of 1 cm shows that the grass blades did not influence the measurements. During the tests it was also observed that the grass blades were immediately flattened by the up-rushing waves. The fog filter and recording of all echoes also gave decent results, as these settings do not influence the results much during dry weather conditions. However, the tests with a higher frequency and higher resolution gave much worse results, because the higher frequency of 100 Hz comes at the cost of interlacing and a coarser resolution (0.667°), which led to coarse results and was not sufficient to capture the run-up peaks accurately. The same holds for the higher resolution, which is also achieved by interlacing.

Rain was simulated with two garden sprinklers placed on top of the ‘flume’ walls, see Fig. 3. In general, the rain deteriorated the quality of the data, resulting in larger percentages of filtered out points and larger threshold values. The ‘normal’ raindrops tended to not be visible nor influence the data, only the strong and continuous beam of water close to the sprinkler was visible in the results.

This indicates that normal rain would influence the results only slightly or not at all. With rain, using the first echo led to more detection of rain, as the beam sometimes reflected off a raindrop. Using the last echo or all echoes improved the results, as these later echoes did come from behind the raindrops. Using the particle filter seemed to remove some of the raindrop echoes from the data as well. Using the fog filter during rain led to much worse results, possibly by too strong filtering, and is not recommended. In general, during rain the best results were achieved with the last echo. A combination of the last echo and particle filter or all echoes could be used as well, but the latter will lead to five times larger data files.

Wind induced vibrations were simulated by manually shaking the guy-wires with which the pole was secured, see Fig. 3. It must be noted that for this temporary set-up there was still slack on the lines and that they could be secured more tightly when the system is placed for a whole storm season. The translations and rotations of the laser scanners were recorded with an accelerometer, as visible in Fig. 3. Even with the slacking lines and strong movements of the lines, the resulting displacement of the laser line in any direction was not more than 5 cm and did not significantly influence the data quality or run-up results. With a more permanent placement during a storm season, the lines could be tightened more, and vibrations should be largely eliminated. However, it would still be good to attach the accelerometer, to be able to correlate possible outliers during a storm with potentially occurring vibrations.

Fig. 3. Left: Simulation of rain with garden sprinklers. Right: Laser scanners with guy-wires and accelerometer (circle).

4.2 Results and analysis of normally incident waves

4.2.1 Wave run-up

The left panel of Fig. 4 shows the run-up heights for test 1 from both laser scanners and based on both the distance and RSSI data plotted against the visually observed run-up heights taken from video data. 15 out of 21 waves are visible, as waves with a filling level of 6 and 7 m overtopped the dike. It is visible that the data correspond well, most data lie within the 5% bounds and all data lie within the 10% bounds. The run-up was simulated in a robust manner, as the run-up levels for each set of three waves with the same filling level lie within a few cm of one another. The data of both laser scanners lie quite closely together, with laser scanner 2 giving a somewhat larger RMSD (root-mean-square deviation, also known as root-mean-square error, RMSE) from the observed data. For this case, determining the run-up based on the distance and RSSI gave almost equal results. This is an improvement compared to what was found in Hofland et al. (2015) and Cete (2019), where the RSSI performed better. This can be explained by the lower layer thickness threshold of 1 cm that was used here, a result of the extensive calibration of the system. The differences that do occur between both laser scanners and between the lasers and video were caused by the variability over the width of the front of the up-rushing wave, since the average run-up height of the front was taken from the video data, and since the laser data give the run-up at two specific locations along the front. The variability in the 2% run-up height ($R_{u2\%}$) over the width of the flume (excluding wall effects) was determined as on average 7% of the $R_{u2\%}$ for tests in the Delta Flume (Cete, 2019). Although smaller, oscillations over the width were also visible in the videos of the present tests.

The right panel of Fig. 4 gives the results for test 1a, with 100 randomly generated waves. Of this test, only 81 waves could be used, as someone blocked the laser beam during the last waves of the test. As no video recording was available for this case, the laser data were compared against the Rayleigh distributed relation between the run-up height and the filling level of the simulator, as determined for this specific location. The x-axis on Rayleigh scale such that deviations from the Rayleigh scale are easily recognized. The data correspond quite well to a Rayleigh distribution for the higher run-up levels. One outlier is visible in the RSSI-values of laser 1. For the highest few run-up levels a more horizontal behaviour was found. This was caused by the fact that the largest waves overtopped the dike, which means that the maximum measured run-up level was the crest level of the dike (dashed line). The lowest run-up levels were higher than what was expected according to the Rayleigh distribution. The equation was fitted based on visual observations of the 3*7 different waves during a calibration test. During the test with the laser scanners, it was also observed that the run-up was higher than during the test on which the relation was based. Some uncertainty exists in the amount of water in the tank, as the waves were generated at the moment that a person at the run-up simulator saw that the required filling level was reached.

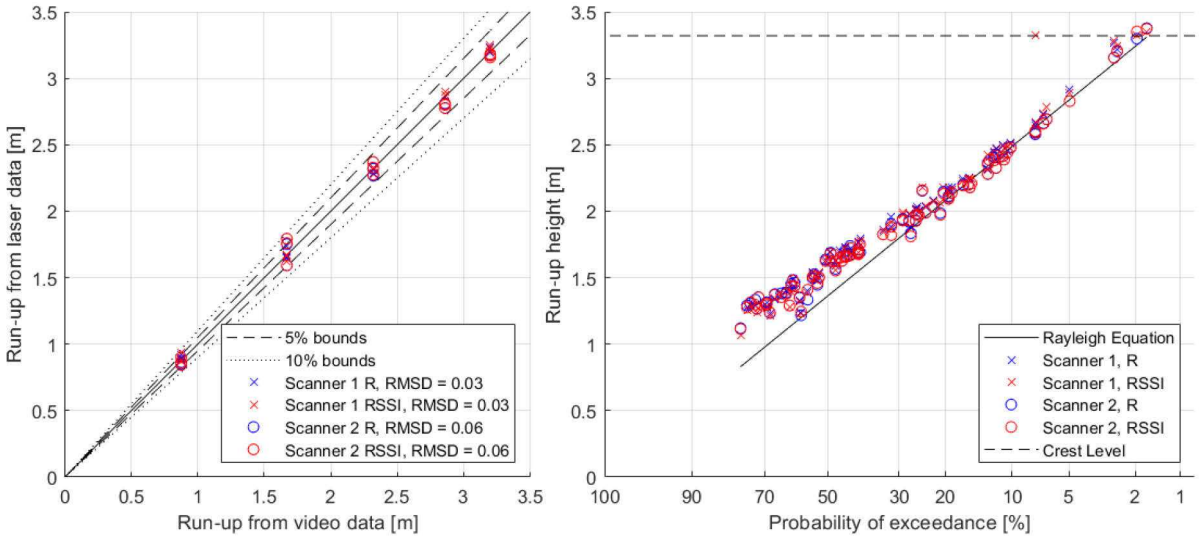

Fig. 4. Left: Run-up data for test 1 from both laser scanners and based on both distance and RSSI versus run-up heights from video data. Right: Run-up data for test 1a from both laser scanners and based on both distance and RSSI, as well as Rayleigh distribution from wave run-up simulator filling level formula. The x-axis on Rayleigh scale, the crest level of the dike is indicated with the horizontal dashed line.

4.2.2 Layer Thickness

As mentioned before, the layer thickness was also measured by five 'surf boards' (floaters). The left panel of Fig. 5 compares the maximum layer thicknesses of the different waves as measured by the laser scanners at a height of z = 1.42 m on the slope with the surf board at this same location, as well as with visually estimated layer thicknesses and with the linear equation $h = c_h(R_u - z)$ from Van der Meer (2011), with h the layer thickness [m], c_h a coefficient, in this case being 0.25 [-] (for a 1:5 slope), R_u the run-up height [m], and z an arbitrary height on the slope [m]. Note that the lines are curved here, since the equation was not plotted against the run-up level, but the corresponding filling level of the simulator.

At this location, the data correspond quite well, with an RMSD of 9 cm between the surf board and the visually estimated values (see legend of Fig. 5). Here, the RMSD between surf board and laser scanners was 7 cm (see title of figure) and between visually estimated values and laser scanners 6 cm (see legend). At this location and higher on the slope, the lasers seem to accurately measure the layer thickness, as the data correspond quite well to the visually estimated and surf board data. At this location, the laser scanners record a somewhat larger layer thickness than the surf board data and for some of the filling levels a somewhat smaller layer thickness than the visually observed data. The laser scanners scan the surface of the foam, which the surf boards do not. Furthermore, it was observed that the surf boards slightly sink into the water and do not record the smallest layer thicknesses, explaining the somewhat lower layer thicknesses and the zero values for a filling level of

2 m. The shape of the linear equation corresponds quite well, but it overestimates the values. The relation could be used as an upper bound. These trends also hold for locations higher on the slope.

Closer to the simulator, where larger layer thicknesses occurred, different results were found, with larger differences between the different measurement techniques. There, the water was highly turbulent, and a lot of spray and foam occurred. At those locations the visually estimated layer thicknesses lie around 60 or 65 cm for the largest waves (filling levels). As the lasers measure the foam and spray, this led to overestimations of the layer thicknesses (values >1 m were found) close to the simulator for the largest waves. Due to their mounting in the present set-up, the surf boards could not measure a layer thickness larger than approximately 50 cm, and thus gave an underestimation close to the simulator.

The right plot of Fig. 5 shows the layer thickness in time for a wave with a filling level of 7 m at the same location on the slope (z = 1.42 m), for both laser scanners and the surf board. Visible is that the time signal corresponds quite well, but that the lasers give a somewhat larger maximum layer thickness. The same holds for the other waves of the test.

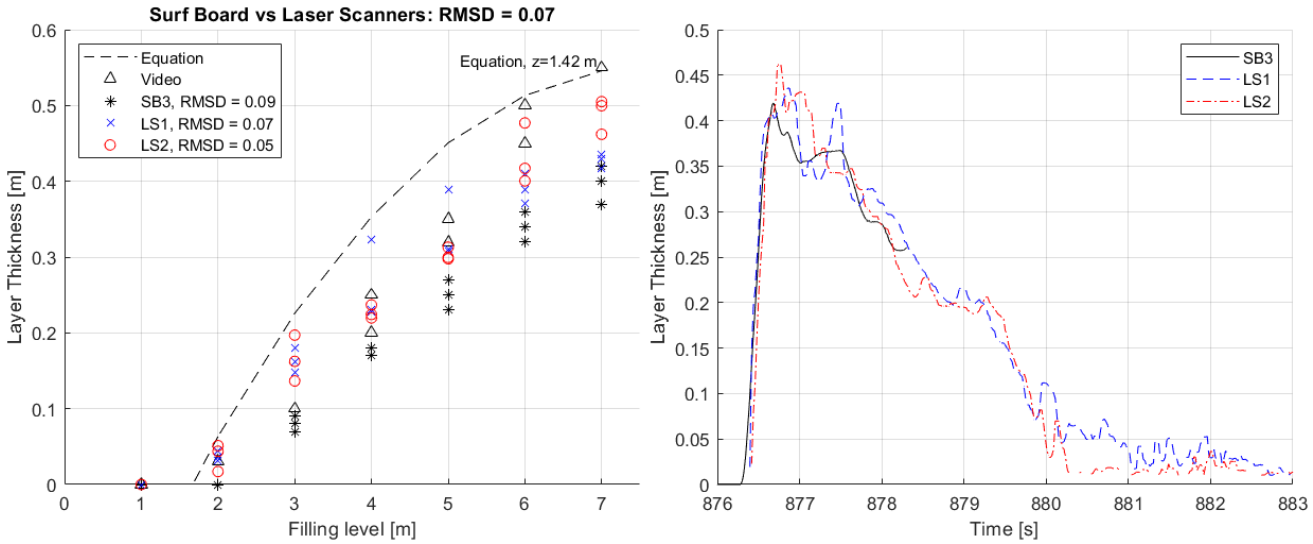

Fig. 5. Left: Layer thicknesses at z = 1.42 m for test 1 as measured with both laser scanners, 'surf boards' and from visual estimations, compared with equation from Van der Meer (2011). Right: Layer thickness in time at the same location for a filling level of 7 m and for both laser scanners and the surf board.

4.2.3 Velocities

The front velocity can be determined by taking the distance the front travels along the slope in a certain period of time or by determining the time derivative of the front displacement. For this, first the displacement along the slope was smoothed by using a median filter with a 0.2 s window and a mean filter with a 0.6 s window, which seemed to give the best results. After that, the time derivative was taken and the maxima were determined, giving the maximum front velocities during each wave. The maximum front velocities were also determined from the videos; by taking the minimum number of video frames it takes the front to travel 1 m.

For these maximum front velocities, there were a few outliers, but most values were within the 10% bounds. The RMSD values were calculated as well. The data points of both laser scanners lie reasonably close together (RMSD = 0.47 m/s), closer than the laser and video data from one another (RMSD = 0.73 m/s). The deviations can be explained by the limited framerate with which the videos were recorded (30 fps), which leads to inaccurate results for large front velocities.

Front velocities were also determined from the videos and the paddle wheel signals by determining the time it takes the front to travel on the slope from one paddle wheel to the next. In the same way, this velocity can also be determined from the laser data. The results are shown in the left panel of Fig. 6. As visible, the data lie closely together, with most data within the 10% bounds, giving confidence in the laser analysis and results. Once again, the RMSD were calculated. The data of both lasers lie closer together (RMSD = 0.28 m/s) than the video and the paddle wheel data to one another (RMSD = 0.30 m/s), giving confidence in the performance of the lasers.

The right panel of Fig. 6 shows the run-up and front velocity time signals of one of the laser scanners and the front velocity time signal from the video analysis for a wave with a simulator filling level of 5 m of test 1. Both the development in time and the maximum front velocity correspond well to one another. The dotted lines indicate percentages of the maximum run-up level. According to Van der Meer (2011), the run-up of a wave starts at a level of 15% of the maximum run-up level, with a front velocity close to the maximum velocity, and this velocity is more or less constant until a level of 75% of the maximum run-up level. The real maximum front velocity is reached between 30%-40% of the maximum run-up level. As visible in Fig. 6, the highest front velocities indeed occur within the range of 15%-75% of the maximum run-up level. In this case, the actual peak of the front velocity is reached just after the 40% line. This also holds for the other waves of this test. This difference in location of the peak front velocity can be explained by the fact that the analysis of Van der Meer (2011) was based on real waves instead of waves generated by the wave run-up simulator. Despite this deviation in peak location, the wave run-up simulator seems to properly simulate the development of the front velocity of a wave. The erratic development of the run-up signal during the run-down of the wave can be explained by the very small layer thicknesses that occur during the run-down, which lie around the used threshold value for the layer thickness.

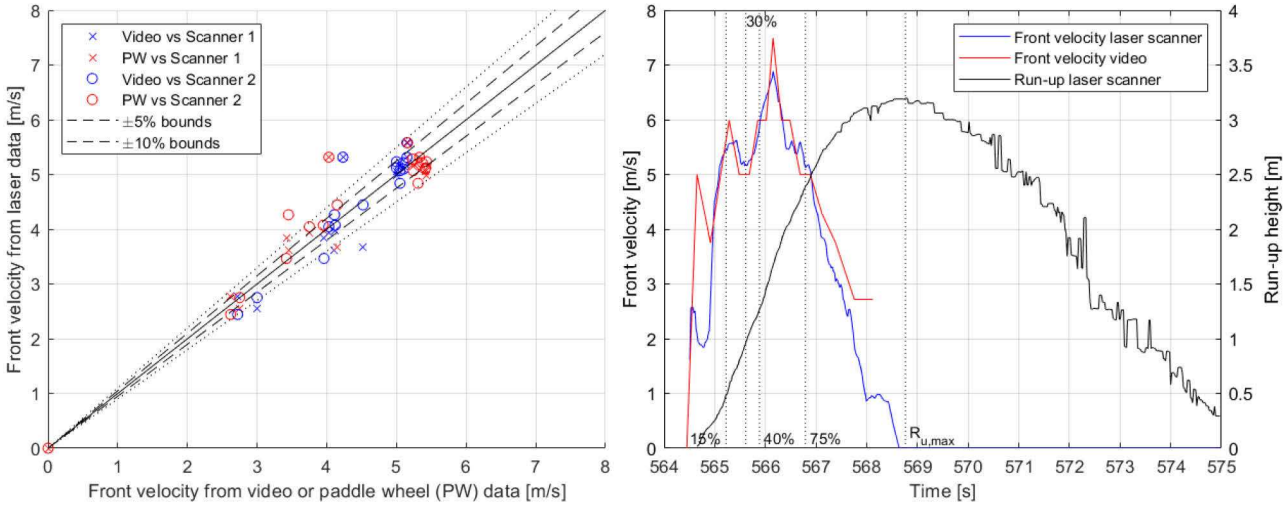

Fig. 6. Left: Front velocities from laser data compared to video and paddle wheel (PW) data. Right: Run-up and front velocity time signals of one of the laser scanners and front velocity time signal from video analysis for a wave with a filling level of 5 m of test 1. Dotted lines indicate percentages of the maximum run-up level.

4.2.4 Wave overtopping volumes and discharge

The (virtual) wave overtopping volumes and mean discharges can be calculated at different virtual crest levels by determining the volume above this crest level by integrating the layer thickness. The overtopping volumes were then found by taking the maximum values of these volumes during each wave. It was assumed that these maximum volumes per wave corresponded to the overtopping volumes. The mean overtopping discharge (q, in m^3/s per m width) was then found by taking the sum of the volumes and dividing by the duration of the test, $q = \sum_N V / D$, with N the number of waves, V the volumes above the virtual crest level [m^2] and D the duration of the test [s]. The virtual overtopping discharge was also calculated by multiplying the front velocity time series with the layer thickness time series at several virtual crest heights. Here, the assumption was made that the front velocity corresponded to the flow velocity at the virtual crest. The left panel of Fig. 7 shows the results for test 1a and compares them with the EurOtop (2018) wave overtopping equations.

Visible is that the discharges based on the maximum volumes correspond very well to the EurOtop (2018) equations. Good results were achieved before for wave flume tests by determining the overtopping using the sum of the volumes above a virtual crests (Hofland et al., 2015; Cete, 2019), but the method had not been applied to an actual dike before.

The method of multiplying front velocity with layer thickness has not been applied before. Even though the assumption of local velocity equals front velocity was used, for this case results were found that are mostly within the 90% bounds, but clearly deviating from the mean line.

The differences that occurred could have several causes. One cause could be that the laser scanners detect a too large layer thickness, caused by foam on top of the water. The overtopping analysis was

run again, now removing 10% of the local layer thickness, assuming this was foam and water aeration. This did not change the overall results significantly, but could be of influence for the lower freeboards, as there was a lot of foam and aeration close to the simulator. Another likely cause is that only filling levels larger than 0.7 m were simulated, which means that the smallest waves were omitted. This can explain the slightly lower discharges that were found for the lowest crest freeboards, as these small waves would contribute to the overtopping for these low freeboards. Despite the fact that these results were based on only 81 waves, since for the calculation of overtopping discharges usually much larger numbers of waves are used, the results correspond well to the EurOtop (2018) equations. Furthermore, even though the wave run-up simulator is calibrated on run-up levels and not on overtopping volumes or discharges, the results for this case correspond very well to the most commonly used overtopping equations.

The results of both laser scanners lie closely together. Only for the largest crest freeboards slight deviations occur, because these overtopping discharges were only based on a few waves. As mentioned before, there was variability in the run-up height over the width of the 'flume'. If a wave surpasses the crest height at the scan transect of laser scanner 1, but barely reaches the crest at the transect of laser scanner 2, this quickly results in a different overtopping discharge for these high freeboards.

The right panel of Fig. 7 shows the distribution of (virtual) overtopping volumes, compared with the EurOtop (2018) equations that give the overtopping volume for a certain probability of exceedance. It is clearly visible that the volumes correspond well for the medium and high crest level. For the lower crest level, the data correspond well for the larger probabilities of exceedance, but for the smaller probabilities (larger volumes) the volumes are lower than according to the equation. For these low freeboards, a large virtual overtopping volume means that a large layer thickness was present over a large area of the slope. If there is any bias or error in the layer thickness as determined by the laser scanners, this error starts to weigh stronger for these low freeboards and large volumes, because of the large surface that is integrated. Furthermore, the run-down, which does not occur with an overtopping tank, could play a role. As mentioned before, the limited number of waves in the record could also be of influence.

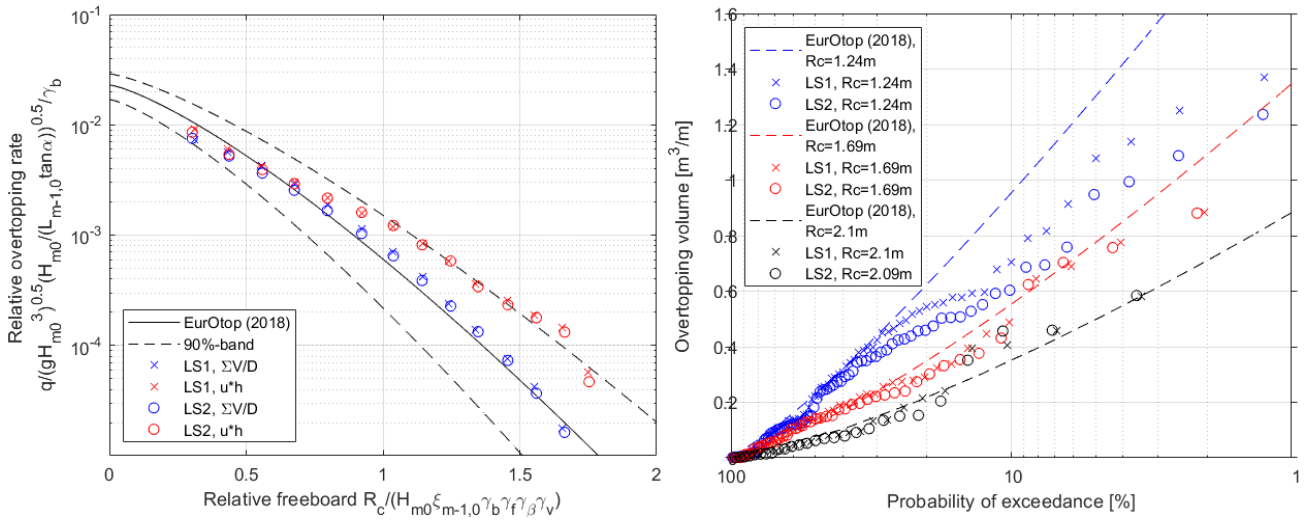

Fig. 7. Left: Relative overtopping rate for several virtual crest levels for test 1a and based on maximum volumes or layer thickness multiplied with front velocity, compared to EurOtop (2018) equations. Right: Distribution of individual overtopping volumes, compared to EurOtop (2018). R_c is the crest freeboard [m], $\xi_{m-1,0}$ is the breaker parameter [-], the different γ parameters are influence factors [-], see EurOtop (2018).

5 Outlook obliquely incident waves and other parameters

In next steps of the study, the data of all tests with normally incident waves will be analysed in more detail, as well as the data of the tests with oblique waves. Fig. 8 shows a snapshot of both laser scanners during oblique wave attack. The time lag and different maximum run-up levels are clearly visible. From the cross-correlation between the two measured signals, potentially the 3D front velocity and direction can be determined and the overtopping volumes and discharges calculated.

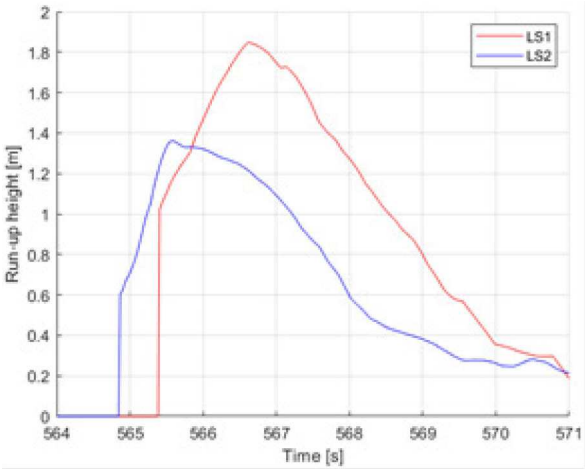

Fig. 8. Snapshot of run-up level in time for both laser scanners during oblique wave attack. The time lag and different maximum run-up levels are visible.

6 Conclusions

This paper presents the successful implementation of an innovative system to measure wave run-up and calculate overtopping using two coupled laser scanners at a field site. The system can determine the layer thicknesses and front velocities on a dike. The paper considers the first tests with the system, with normal and oblique waves generated by the wave run-up simulator on the grass slope of a dike. A range of environmental conditions was simulated, to determine their influence on the measurements.

The ideal laser scanner settings were determined for both dry and rainy conditions. Using the last echo gave the best results and is especially important during rainy conditions. The influence of vibrations of the laser scanners due to wind on the data quality and run-up results was small. With a more fixed placement of the system during a storm season, vibrations should be largely eliminated. However, it would still be good to attach an accelerometer to be able to correlate possible outliers during a storm with potentially occurring vibrations.

The resulting run-up heights corresponded well to the visually observed run-up, with differences of only a few cm, both for the run-up based on measured distance and based on laser reflectance. Layer thicknesses were determined as being reliable with the laser scanners as well as with a commonly used method (‘surf boards’) for locations higher on the dike slope. Closer to the simulator, the lasers gave too large and unreliable layer thicknesses due to foam and spray. The advantage compared to the surf boards is that the layer thickness can be determined over the whole slope, not just at a few locations.

The front velocities were also determined as being reliable from the laser scanner data as well as from the commonly used method of displacement of the front in a certain time period (based on video and paddle wheel data). The average front velocities between two paddlewheels corresponded quite well with the velocities as determined from the videos and paddle wheels. Furthermore, the development in time and the maxima of the front velocities corresponded well with the video results.

The wave overtopping volumes and discharges were calculated at several virtual crest levels. The overtopping discharges based on maximum volumes corresponded very well to the EurOtop (2018) equations, although more research is recommended. The discharges based on layer thicknesses multiplied with front velocities corresponded less well, although with most values within the 90% bounds of the overtopping equations.

For this case, the wave run-up, layer thickness and front velocities could be determined accurately with the laser scanner system as well as with the conventionally used methods. Since the system is mobile, it can measure at several dike locations by moving the system every few years.

The goals for the next steps in this study are to determine the 3D front velocity and direction and to calculate the overtopping volumes during oblique wave attack, by considering the correlations between the two measured laser signals.

Acknowledgement

We would like to thank the POV Waddenzeedijken for the use of the wave run-up simulator, as well as Gerben van der Meer, Jan Bakker and Frans Roorda for their help with the wave run-up tests. This study was supported by Waterschap Noorderzijlvest and the Hoogwaterbeschermingsprogramma.

References

Allis, M. J., Peirson, W. L. and Banner, M. L. (2011) 'Application of lidar as a measurement tool for waves', in The Twenty-first International Offshore and Polar Engineering Conference. International Society of Offshore and Polar Engineers.

Blenkinsopp, C. E., Mole, M. A., Turner, I. L. and Peirson, W. L. (2010) 'Measurements of the time-varying free-surface profile across the swash zone obtained using an industrial LIDAR', Coastal Engineering. Elsevier, 57(11–12), pp. 1059–1065.

Cete, C. (2019) Quantifying the effect of woody vegetation on the wave loads on a dike using remote sensing. Large scale physical model tests. Delft University of Technology.

EurOtop (2018) Manual on wave overtopping of sea defences and related structures. An overtopping manual largely based on European research, but for worldwide application. Edited by J. W. Van der Meer, N. W. H. Allsop, T. Bruce, J. De Rouck, A. Kortenhaus, T. Pullen, H. Schüttrumpf, P. Troch, and B. Zanuttigh. Available at: www.overtopping-manual.com.

Hofland, B., Diamantidou, E., van Steeg, P. and Meys, P. (2015) 'Wave runup and wave overtopping measurements using a laser scanner', Coastal engineering. Elsevier, 106, pp. 20–29.

Van der Meer, J. W. (2011) The Wave Run-up Simulator. Idea, necessity, theoretical background and design. Van der Meer Consulting B.V.

Van der Meer, J. W., Schrijver, R., Hardeman, B., van Hoven, A., Verheij, H. and Steendam, G. J. (2010) 'Guidance on erosion resistance of inner slopes of dikes from three years of testing with the Wave Overtopping Simulator', in Proceedings of the ICE, Coasts, Marine Structures and Breakwaters. Edinburgh: Thomas Telford Ltd, pp. 2–460.

Streicher, M., Hofland, B. and Lindenbergh, R. C. (2013) 'Laser ranging for monitoring water waves in the new Deltares Delta Flume', in ISPRS Annals of the photogrammetry, remote sensing and spatial information sciences. Antalya, Turkey: ISPRS.

Valentini, N., Hofland, B. and Saponieri, A. (2014) 'Application of LIDAR as a measurement instrument for laboratory water waves', in Proceedings of Coastlab. Varna, Bulgaria.

Vousdoukas, M. I., Kirupakaramoorthy, T., Oumeraci, H., De La Torre, M., Wübbold, F., Wagner, B. and Schimmels, S. (2014) 'The role of combined laser scanning and video techniques in monitoring wave-by-wave swash zone processes', Coastal Engineering. Elsevier, 83, pp. 150–165.